hydrology

MDPI

Article

Projected Changes in Runoff, Groundwater Recharge and Renewable Water Resources in a High-Andean Basin Under Climate Change: A SWAT-CMIP5 Modeling Approach

Jhonatan Hinojosa Mamani [1], Benito Pepe Calsina Calsina [1,*], Yalmar Temistocles Ponce Atencio [1], Juan Manuel Tito Humpiri [1], Henry Pizarro Viveros [1] and Maribel Erika Cahuana Huichi [2]

[1] Faculty of Management and Social Sciences, National University of Juliaca, Juliaca 21100, Peru
[2] Faculty of Education, National University of the Altiplano, Puno 21001, Peru
* Correspondence: bpcalsinac.doc@unaj.edu.pe

Abstract

Climate change is expected to significantly alter hydrological regimes in high-altitude tropical basins, where water availability strongly depends on precipitation variability and groundwater processes. The Ramis River basin, a major tributary of Lake Titicaca in the Peruvian Altiplano, is particularly vulnerable to hydroclimatic variability due to its dependence on seasonal water resources. This study evaluates the impacts of climate change on runoff, groundwater recharge, percolation, and renewable water resources using the SWAT hydrological model calibrated and validated for the period 1981–2024. Future projections were developed using the MPI-ESM-MR and ACCESS1-0 global climate models under RCP 4.5 and RCP 8.5 scenarios for the period 2025–2100, applying bias correction through CMhyd. The results indicate a strong sensitivity of basin hydrology to climate forcing. Under the MPI-ESM-MR model, runoff decreases by up to 68% under RCP 4.5, while extreme increases exceeding 130% are projected under RCP 8.5. In contrast, ACCESS1-0 shows moderate reductions in most scenarios. Renewable water resources exhibit a general declining trend (−23% to −41%), suggesting increasing water scarcity conditions. Additionally, the Standardized Precipitation Index (SPI) reveals a higher frequency and persistence of drought events toward the end of the century, particularly under high-emission scenarios. Overall, the findings indicate that the Ramis River basin may face a dual hydroclimatic risk characterized by reduced water availability and increased hydrological extremes. These results highlight the need to integrate climate projections into water resource management and to implement adaptive strategies to reduce future water vulnerability in high-Andean basins.

Keywords: climate change; hydrological modeling; water stress; SWAT; standardized precipitation index

Check for updates

Academic Editor: Ioannis Panagopoulos

Received: 1 April 2026
Revised: 9 May 2026
Accepted: 11 May 2026
Published: 17 June 2026

Copyright: © 2026 by the authors. Licensee MDPI, Basel, Switzerland. This article is an open access article distributed under the terms and conditions of the Creative Commons Attribution (CC BY) license.

1. Introduction

Climate change is increasingly recognized as a dominant driver of hydrological variability, particularly in high-altitude tropical basins where small shifts in temperature and precipitation can produce disproportionate impacts on water availability and ecosystem stability [1–4]. These regions are especially sensitive due to their strong dependence on seasonal precipitation, cryospheric contributions, and complex topographic controls, which amplify hydroclimatic responses to global warming [5–7]. As a result, alterations

in precipitation patterns and rising temperatures are expected to significantly affect key components of the hydrological cycle, including runoff generation, evapotranspiration, groundwater recharge, and overall water balance [8–10].

In the Andean region, and particularly in the Peruvian Altiplano, water resources are highly vulnerable to climate variability and change. The Ramis River basin, one of the main tributaries of Lake Titicaca, plays a crucial role in regional water supply for agriculture, livestock, and human consumption. However, increasing climate variability has intensified hydrological extremes such as floods and droughts, affecting water availability and ecosystem resilience [11–13]. Historical evidence indicates that extreme hydrological events in the Altiplano are closely linked to large-scale climatic drivers, including El Niño–Southern Oscillation (ENSO), which significantly modulates precipitation and runoff patterns in the region. Climate scenario frameworks have evolved from representative concentration pathways (RCPs) to shared socioeconomic pathways (SSPs), allowing the integration of radiative forcing trajectories with assumptions about future development patterns. CMIP6 simulations consistently project regional warming exceeding 1.5 °C under intermediate scenarios and more than 2 °C under high-emission pathways by the end of the century [14–16].

To assess the impacts of climate change on hydrological systems, physically based models such as the Soil and Water Assessment Tool (SWAT) have been widely applied due to their ability to simulate spatial and temporal variability of hydrological processes under different climatic and land-use scenarios [17–19]. As a consequence, future hydrological conditions may not only depend on precipitation changes, but also on the interaction between warming, evapotranspiration, and land-surface processes, which together control the availability of renewable water resources. SWAT is particularly suitable for data-scarce regions like the Andes, as it allows the integration of multiple data sources and supports long-term simulations of water balance components [20–22]. Additionally, the incorporation of climate projections derived from Global Climate Models (GCMs), such as those included in CMIP5, enables the evaluation of future hydrological responses under different greenhouse gas emission scenarios, including RCP4.5 and RCP8.5 [23–25].

Recent studies have demonstrated that climate change may lead to significant alterations in runoff regimes, groundwater recharge, and sediment transport in mountainous basins, with implications for water resource management and sustainability [26–28]. However, despite these advances, there remains a lack of integrated assessments that simultaneously evaluate runoff, groundwater processes, and renewable water resources in high-Andean basins. In particular, few studies have addressed long-term changes in water availability and drought dynamics using combined hydrological modeling and climate projections in the Ramis River basin.

Therefore, this study aims to quantify the impacts of climate change on runoff, groundwater recharge, percolation, and renewable water resources in the Ramis River basin using a SWAT–CMIP5 modeling framework. Future projections are developed using the MPI-ESM-MR and ACCESS1-0 models under RCP4.5 and RCP8.5 scenarios for the period 2025–2100. In addition, drought dynamics are evaluated using the Standardized Precipitation Index (SPI) to assess the frequency and severity of extreme hydroclimatic events. The findings of this study are expected to provide relevant insights for water resource management and climate adaptation strategies in high-altitude Andean basins. Although previous studies have addressed hydrological responses in other Andean basins, this research specifically focuses on the Ramis River basin, which presents distinct hydroclimatic characteristics, including high-altitude variability, glacier influence, and unique precipitation patterns. Therefore, this study provides a basin-specific assessment that contributes to a more comprehensive understanding of climate change impacts on water resources in the Peruvian Altiplano.

2. Materials and Methods

2.1. Study Area

This study was conducted in the Ramis River basin, located in southern Peru and northern Puno region, covering an area of 14,684 km^2, with a maximum altitude of 5750 m above sea level at Cerro Sur Puna and a minimum altitude of 3802 m above sea level at its mouth on Lake Titicaca. Geographically, it extends across the basin extends UTM coordinates 18L, Northing 8,289,725–8,445,867 m and Easting 272,732–454,221 m, as illustrated in Figure 1.

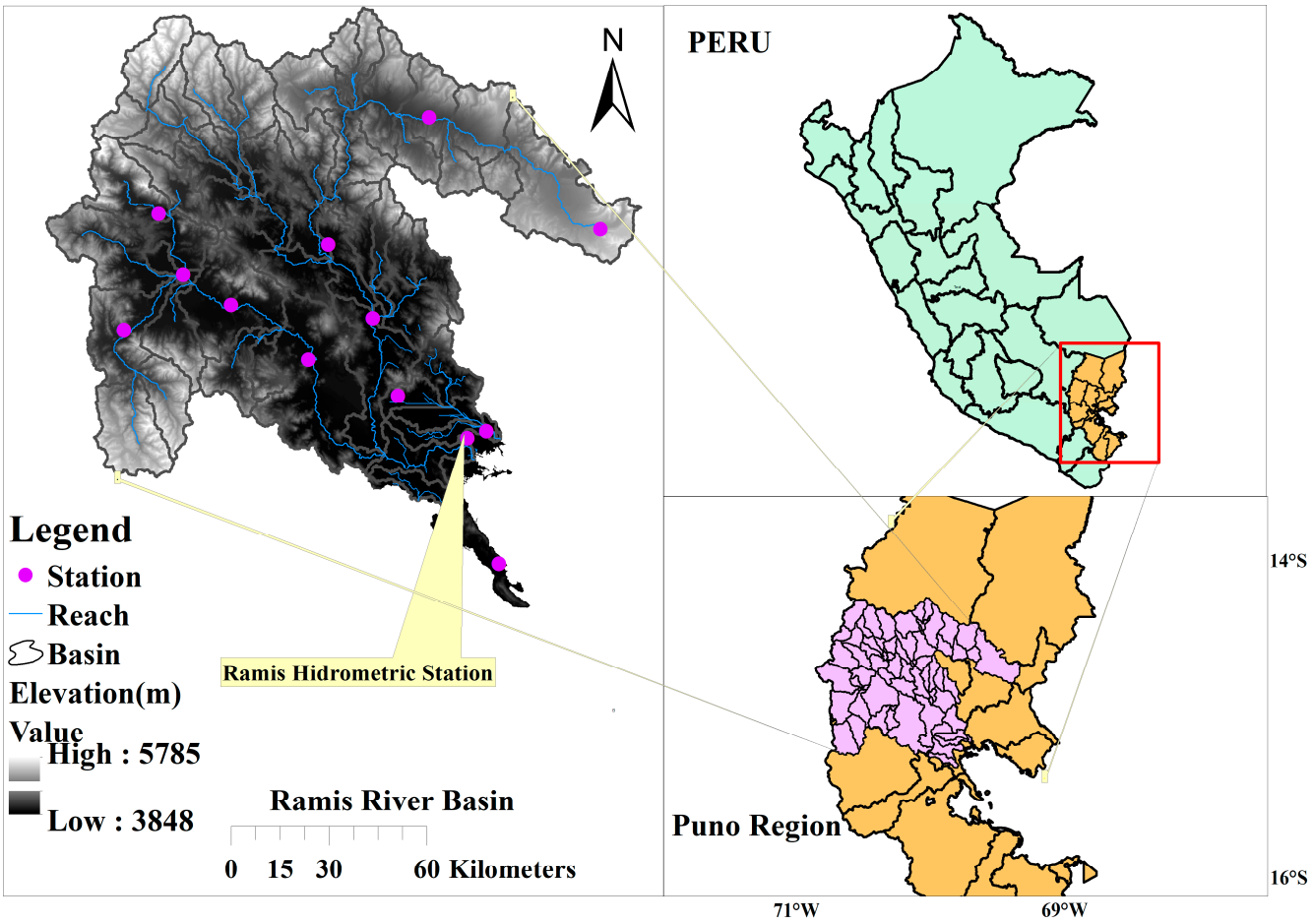

Figure 1. Location and spatial configuration of the Ramis River basin.

The Ramis River basin originates at the confluence of the Azángaro and Ayaviri rivers, from where the river system takes the name Ramis until it flows into Lake Titicaca. Its main course extends approximately 320 km from the high-Andean punas to its final discharge into the lake, making it one of the main water sources in the northern sector of the Titicaca system. Before reaching the lake, there is the Ramis Road Bridge hydrometric station, monitored by SENAMHI and dated PISCO V2.1. [22], where the river's flow is monitored. Access to the study area from the city of Puno is via the paved Puno–Juliaca–Ramis highway, a distance of approximately 102 km. The Ramis River basin is bordered to the east by the Ramis and Suches river basins, to the west by the Coata River basin, to the north by the interior high-Andean basins, and to the south by Lake Titicaca.

2.2. SWAT Data

The modeling of the Ramis River basin was based on the implementation of the SWAT algorithm [23], integrating high-precision geospatial and climatic inputs for a detailed

characterization of the territory. Using a 90 m Digital Elevation Model (DEM) provided by the Alaska Satellite Facility, topographic delimitation and drainage network configuration were carried out in a GIS environment, complemented by FAO soil mapping and USGS vegetation cover data. This structure allowed the study area to be segmented into 68 sub-basins, which in turn were disaggregated into 2902 Hydrological Response Units (HRUs) as shown in Figure 2, defined by a unique combination of soil, slope, and land use variables thus ensuring a spatially explicit simulation of regional water dynamics.

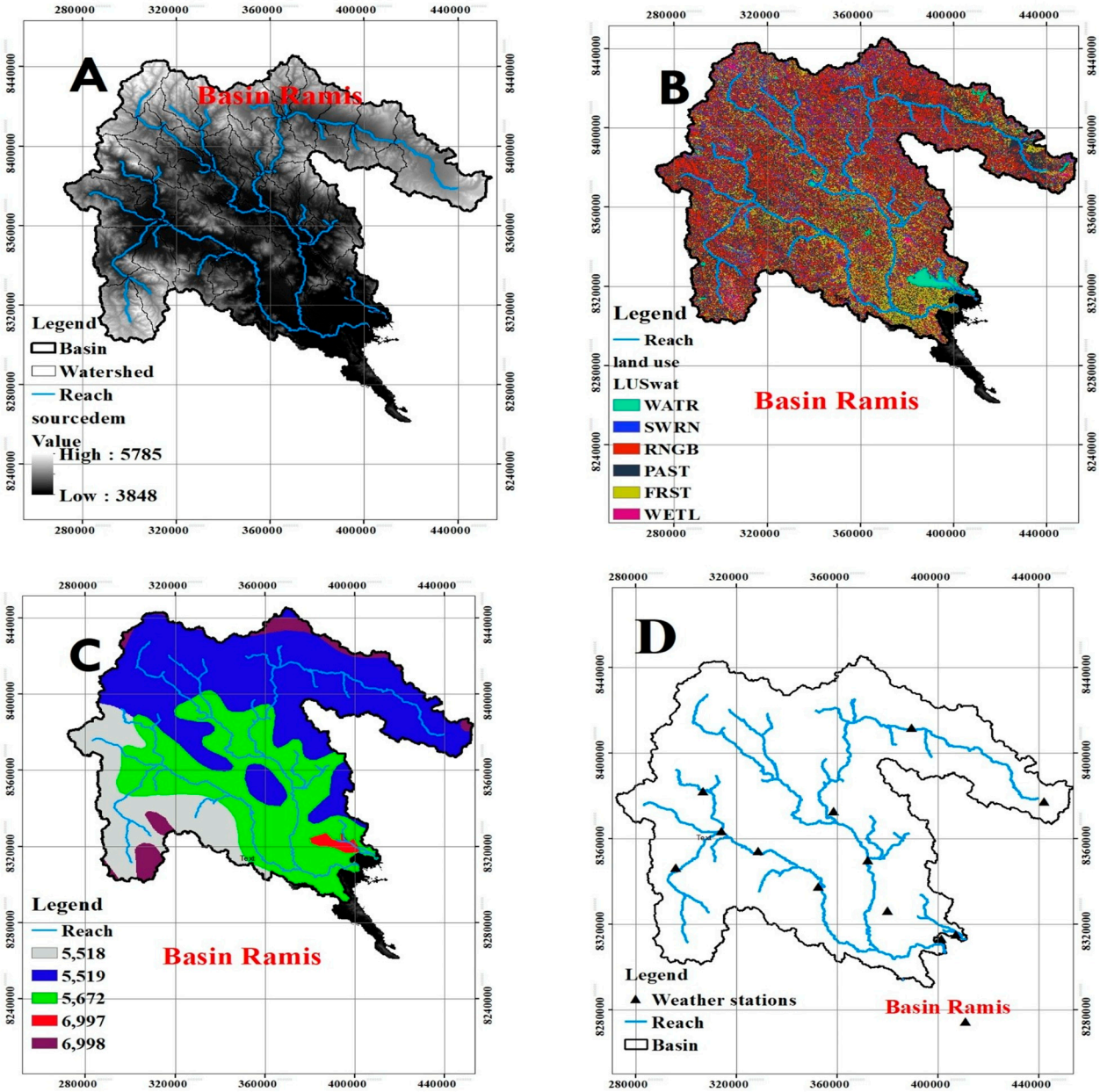

Figure 2. Digital Elevation Model (DEM) (**A**), land use (**B**), soil map (**C**), weather stations (**D**).

The forcing configuration of the SWAT model (v. 2012) integrated daily historical series of precipitation and extreme temperatures (minimum and maximum) from six weather stations for the period 1981–2024. The computational environment was structured on ArcGIS 10.8.26, allowing for a robust representation of surface hydrological processes. To ensure the reliability of the simulations, a calibration and validation process was performed on a monthly basis, comparing the model outputs with the flows observed at the Ramis road bridge hydrometric station (specifications in Table 1). This parametric adjustment was

performed using the SUFI-2 optimization protocol integrated into the SWAT-CUP platform, ensuring the minimization of uncertainty in the estimation of the basin's water balance.

Table 1. Geospatial parameters of the hydrometric station.

Station	Station Code	Altitude(m)	Longitude (W)	Latitude (S)
Puente Carretera Ramis	47251282	3812	69°52′25.7″	15°15′19.6″

2.3. Configuration of Annual Scenarios Through the Forcing of General Circulation Models

In order to quantify the hydroclimatic response of the basin to various radiative forcings the General Circulation Models (GCMs) MPI-ESM-MR and ACCESS1-0, integrated into the CMIP5 project, were selected due to their performance in representing regional climate dynamics [29,30]. The analysis was based on the representative concentration pathways RCP 4.5 and RCP 8.5, which describe scenarios of intermediate stabilization and high emissions, respectively [24,25].

Given the original resolution of the GCMs, the precipitation and temperature time series were subjected to a post-processing protocol using the CMhyd tool (v1.0). This procedure included extraction, spatial disaggregation, downscaling, and bias correction, ensuring statistical consistency between the simulated data and historical observations [27,28]. This methodology has proven effective in mitigating the systematic discrepancies inherent in global climate projections in various regions [28] as shown in Table 2. Finally, the adjusted daily dataset was integrated as a forcing factor into the SWAT model, allowing for a comparative assessment of the hydrometeorological trends projected for the 2025–2100-time horizon.

Table 2. Global socioeconomic and atmospheric indicators: Comparison between the base year (1990) and projections of RCP 4.5 and 8.5 trajectories to the year 2100.

Scenario Characteristics	1990	RCP 4.5	RCP 8.5
World Population (Millions)	5.3	9.3	12.0
CO_2 Concentration (ppm)	354	538	936
Global GDP (trillion USD, PPP)	23	250	300

2.4. Execution of the SWAT Model

The Soil and Water Assessment Tool (SWAT) is a physically based, continuous-time, semi-distributed simulation tool designed to predict the impact of soil management practices on hydrological regimes, sediment transport, and agrochemical dynamics in highly complex watersheds [23,30–32]. Based on this data, it indirectly simulates physical processes such as water flow, sediment transport, plant growth, and nutrient cycling using defined input parameters.

The model is computationally efficient and allows for the simulation of long-term processes such as erosion and nutrient cycling. Surface runoff is estimated using the Soil Conservation Service (SCS-CN) curve number method, which also integrates lateral flow, snowmelt, and aquifer recharge processes. The SWAT model is based on the fundamental water balance Equation (1), which governs the distribution and storage of water in the soil profile and allows the simulation of hydrological fluxes [33].

$$SW_t = SW_a + \sum_{t=1}^{t} (R_d - Q_s - E_a - W_{seep} - Q_{gw}) \quad (1)$$

where SW_t (mm) denotes the total water content in the soil, SW_a (mm) is the initial soil moisture level, and t represents time expressed in days. R_d is the daily precipitation,

while Q_s (mm) refers to the surface runoff generated. E_a is the actual evapotranspiration, W_{seep} (mm) is the volume of water that infiltrates into the unsaturated zone (vadose zone) during day t, and Q_{gw} (mm) indicates the return flow or underground runoff that occurs on that same day t.

2.5. Sensitivity Analysis and Model Calibration

Given the high parametric dimensionality of the SWAT model and the complexity of the simulated hydrological interactions, the SWAT-CUP (SWAT Calibration and Uncertainty Programs) protocol was used to optimize the system [34,35]. The process began with a global sensitivity analysis, which allows the relative influence of each parameter to be identified by simultaneously evaluating their variations, unlike local analysis, which is restricted to adjusting variables in isolation. The statistical significance of the parameters was determined using the t-statistic and the *p*-value; those with higher absolute values of t and significance levels close to zero were identified as the main drivers of the model's response [36,37]. After identifying the critical parameters, the model was calibrated to minimize the discrepancy between simulated and observed values. The goodness of fit and predictive capacity of the model were evaluated using robust performance metrics, specifically the coefficient of determination R^2 and the Nash–Sutcliffe efficiency index (NSE), thus ensuring the representativeness of the hydrological processes in the basin.

2.6. Standard Precipitation Index (SPI)

The Standardized Precipitation Index (SPI), originally proposed by McKee et al. [38], is a meteorological drought indicator based exclusively on precipitation data. It is widely used to quantify rainfall anomalies and identify periods of water deficit or excess across different climatic regions and temporal scales [39]. Due to its robustness and spatial comparability, SPI has been adopted by the World Meteorological Organization (WMO) as a standard tool for drought monitoring [40]. In this study, SPI was computed at the 12-month accumulation scale (SPI-12) to evaluate long-term hydroclimatic variability. For the historical period, SPI was calculated using observed precipitation data, while for future scenarios it was derived from bias-corrected CMIP5 precipitation projections.

The SPI is calculated by fitting a probability distribution to long-term precipitation data and transforming it into a standard normal distribution with zero mean and unit variance [40]. This transformation allows SPI values to be interpreted as standardized deviations from the climatological mean, facilitating the identification of extreme wet and dry conditions, following Equation (2).

The SPI is defined as

$$\mathrm{SPI} = \frac{X_0 - X^-}{S_n} \tag{2}$$

X^- is the average precipitation per month, S_n is the standard deviation on the time scale, and X_0 is the rainfall per month.

Given the stochastic nature and normalization of the SPI, this index allows for bimodal monitoring that covers both the humidity spectrum and the water deficit spectrum with a unified metric. The structure of the SPI facilitates the identification of the severity of extreme events based on the standard deviation from the historical median. Table 3 details the classification scheme proposed by McKee et al. [38], which segments climatic states based on specific probability thresholds, allowing for a standardized interpretation of the intensity of droughts and rainy periods.

Table 3. Classification of hydroclimatic conditions based on SPI values.

SPI		Probability (%)
SPI $\geq$ 2.0	Extremely wet	2.3
1.5 $\leq$ SPI $<$ 2.0	Very wet	4.4
1.0 $\leq$ SPI $<$ 1.5	Moderately wet	9.2
$-1.0 <$ SPI < 1.0	Close to normal	68.2
$-1.0 \geq$ SPI > -1.5	Moderately dry	9.2
$-1.5 \geq$ SPI > -2.0	Severely dry	4.4
$-2.0 \geq$ SPI	Extremely dry	2.3

3. Results

3.1. Analysis of the Variability of Model Parameters

The hydrological response observed in the Ramis River basin differs from patterns reported in other Andean catchments, highlighting the importance of localized analyses when assessing climate change impacts. The period between 1981 and 2024 was selected following a statistical analysis of data from weather and hydrometric stations in the studied basin, also considering the research objectives and the need for modeled inputs in continuous and simultaneous time series. Within this interval, the years 1981–2016 were used for the calibration phase, while the last three years (2017–2024) were used for model validation.

To calibrate and validate the SWAT model, monthly time series of observed data were prepared and parameter runoffs were analyzed using SWAT-CUP (v5.1.6.2) software together with the SUFI-2 algorithm.

The parameters with the greatest impact on flow are presented in Table 4. Regarding the codes used, the letter V indicates the replacement of a parameter with a new value, while the letter R represents the multiplication of the original parameter by (1 + a given value), thus replacing the initial parameter.

Table 4. Sensitivity analysis and determination of effective model parameters; V: replacement of a parameter value with a new value for a new parameter; R: parameter value multiplied by (1 + given value).

Parameter Key	Meaning	T-Stat	*p*-Value
v__CH_N2.rte	Curve number	0.88	0.47
v__ESCO.hru	Soil evaporation compensation factor	−1.76	0.22
v__GW_DELAY.gw	Groundwater delay (days)	0.61	0.61
v__ALPHA_BF.gw	Base flow recession constant	0.38	0.74
v__CH_K2.rte	Effective hydraulic conductivity in main channel floodplain (mm h^{-1})	0.69	0.56
r__CN2.mgt	SCS runoff curve	−0.16	0.89
v__TLAPS.sub	Altitudinal thermal gradient [°C/km]	0.27	0.82

On the other hand, Table 4 shows the effects of various relevant parameters on the simulation of flow in the sub-basins, accompanied by their respective *p*-values and t-stats. Those parameters with a higher absolute t-stat value and a *p*-value close to zero had a greater influence on stream flow.

3.2. Model Calibration and Validation

Following the sensitivity analysis, the model was calibrated and validated by comparing the simulated outputs with the observed monthly flow records. The model's ability to reproduce the hydrological dynamics of the basin was quantified using the coefficient of determination (R^2) and the Nash–Sutcliffe efficiency index (NSE), whose values are summarized in Table 5. As illustrated in the hydrograph in Figure 3, despite the spatial

complexity and surface area of the study unit, the SWAT model demonstrated a remarkable ability to capture seasonal trends and runoff peaks. These results confirm the robustness of the physical parameterization used, ensuring a reliable representation of mass transfer processes in the river system.

Table 5. Evaluation of SWAT model performance using monthly efficiency metrics during calibration and validation periods R^2 y NSE.

Station	River	Station Data	R^2 Calibration	NS Calibration	R^2 Validation	NS Validation
Puente Carretera Ramis	Ramis	2102001	0.84	0.83	0.85	0.82

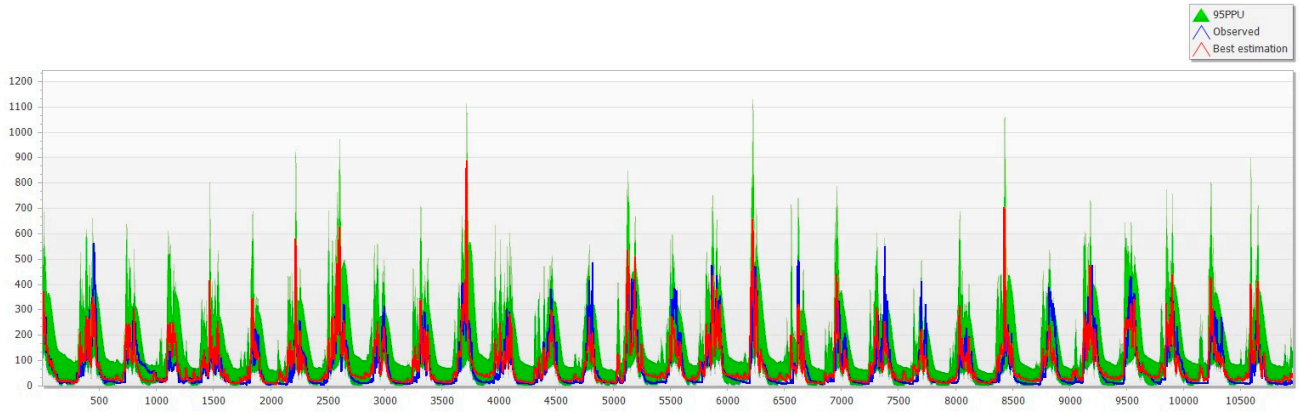

Figure 3. Hydrograph of observed versus simulated monthly flows, including the 95% predictive uncertainty band (95PPU) at the Puente Ramis hydrometric station.

3.3. Evaluation of Peak Flow Simulation

To further evaluate the model performance under extreme hydrological conditions, a peak flow validation analysis was conducted using the highest observed discharge events during the validation period. Figure 4 presents a scatter comparison between observed and simulated peak flows, including a 1:1 reference line.

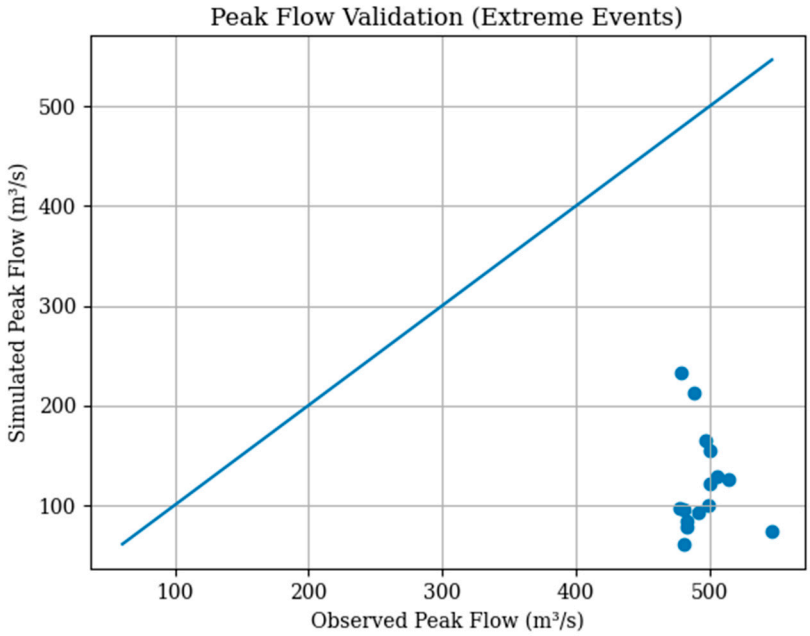

Figure 4. Peak flow comparison between observed and simulated discharge during the validation period.

The results reveal that the SWAT model systematically underestimates peak discharge values. Most simulated peaks fall significantly below the 1:1 line, particularly for high-flow events exceeding 450 m^3/s. This indicates limitations in the model's ability to reproduce the magnitude of extreme hydrological events in the basin.

These discrepancies may be associated with uncertainties in precipitation inputs, spatial resolution limitations, and structural constraints of the model. Therefore, projections of future extreme events, especially under high-emission scenarios (RCP 8.5), should be interpreted with caution.

3.4. Annual Surface Runoff Simulation

The simulation of annual runoff under future climate scenarios reveals a strong dependence of the hydrological response of the Ramis River basin on the structure of the climate model and emission pathway. The historical average discharge for the period 1981–2024 is 47.43 m^3/s, which was used as the reference baseline for evaluating projected changes.

To establish a quantitative link between climate forcing and hydrological response, projected changes in precipitation and temperature were analyzed for both RCP 4.5 and RCP 8.5 scenarios (Table 6). Under RCP 4.5, both climate models show relatively small increases in precipitation (+4.19% for MPI-ESM-MR and +5.54% for ACCESS1-0), combined with moderate temperature increases. These conditions enhance evapotranspiration, leading to a reduction in effective water availability and consequently a decrease in runoff.

Table 6. Projected changes in precipitation and temperature under RCP 8.5 and RCP 4.5.

Model	Scenario	ΔP (%)	(°C)
MPI-ESM-MR	RCP 8.5	+49.3	+3.30
MPI-ESM-MR	RCP 4.5	+4.19	+2.21
ACCESS1-0	RCP 4.5	+5.54	+1.04
ACCESS1-0	RCP 8.5	+7.8	+3.63

In contrast, under RCP 8.5, the MPI-ESM-MR model projects a substantial increase in precipitation (+49.36%), which exceeds evapotranspiration losses and results in a strong amplification of runoff. This explains the transition from negative to highly positive hydrological responses. The ACCESS1-0 model, however, shows only moderate precipitation increases (+7.83%), combined with higher temperature rises, which leads to increased evapotranspiration and reduced runoff. These results demonstrate that the contrasting hydrological responses are driven by differences in climate forcing magnitude and highlight a non-linear relationship between precipitation, temperature, and runoff.

Under this condition, the MPI-ESM-MR model, the RCP 4.5 scenario, shows a pronounced reduction in runoff to 14.89 m^3/s, representing a decrease of approximately 68.6% relative to the historical period. In contrast, the RCP 8.5 scenario produces a marked increase to 110.29 m^3/s, exceeding the historical value by more than 130%.

The ACCESS1-0 model shows a different behavior, with moderate reductions under both scenarios. The projected runoff decreases to 24.73 m^3/s under RCP 4.5 and to 15.99 m^3/s under RCP 8.5, indicating reductions of 47.9% and 66.3%, respectively. These differences between models reflect the high sensitivity of the basin to projected precipitation variability and to the representation of atmospheric processes in global circulation models.

From a hydrological perspective, the reduction observed in several scenarios suggests a potential decrease in effective precipitation and groundwater recharge, which may limit baseflow contributions during the dry season. This condition could increase the probability of seasonal water deficits, particularly in rural areas where water supply depends on surface flow and shallow aquifers. Conversely, the extreme increase simulated by MPI-ESM-MR

under RCP 8.5 indicates a possible intensification of high-flow events, which may increase flood risk and sediment transport in the basin. These results indicate that the future hydrological regime of the Ramis basin may become more irregular as shown in Figure 5 and Table 7, combining periods of reduced water availability with episodes of excessive runoff. Such variability represents a significant challenge for water resource management, as both drought conditions and extreme flows may affect agricultural productivity, infrastructure stability, and ecosystem balance in the northern Altiplano.

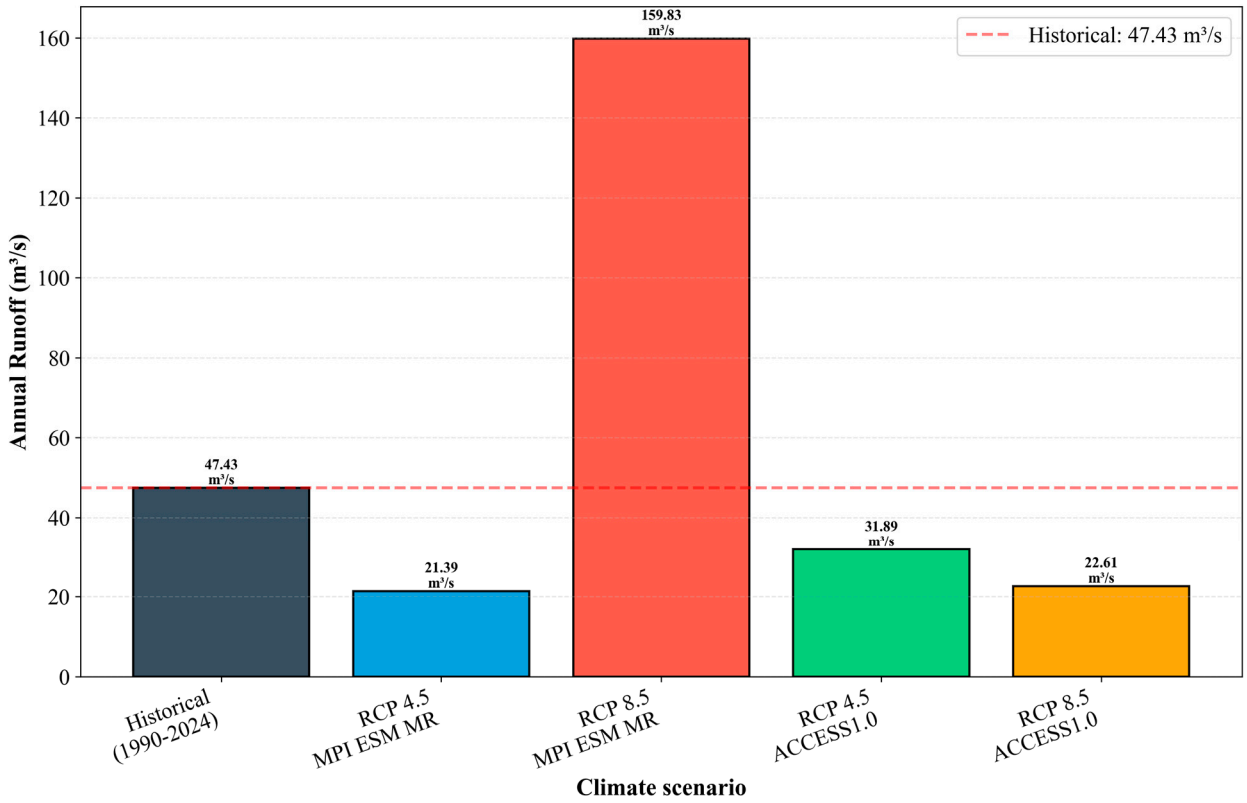

Figure 5. Runoff projections under climate forcing scenarios.

Table 7. Simulation of runoff and surface water under the climate scenarios examined.

Model	Scenario	Period	Surface Water (Mm^3)	Runoff (m^3/s)
Historical			**697.22**	**47.43**
MPI-ESM-MR	RCP 4.5	2025–2100	218.88	14.89
MPI-ESM-MR	RCP 8.5	2025–2100	1621.26	110.29
ACCESS1-0	RCP 4.5	2025–2100	363.53	24.73
ACCESS1-0	RCP 8.5	2025–2100	235.05	15.99

3.5. Time Series Variability Analysis Using ITA and RAPS

To complement the hydrological assessment and provide a deeper evaluation of temporal variability in runoff dynamics, additional analyses were conducted using the Innovative Trend Analysis (ITA) and the Rescaled Adjusted Partial Sums (RAPS) methods. These statistical approaches were applied to the annual runoff series derived from the historical period and future climate projections generated under the MPI-ESM-MR and ACCESS1-0 climate models for the RCP 4.5 and RCP 8.5 scenarios. The objective of these analyses was to identify possible structural changes, temporal irregularities, cumulative anomalies, and long-term variability patterns associated with projected hydroclimatic changes in the Ramis River basin.

The ITA method allows the identification of monotonic and non-monotonic trends without requiring assumptions of normality or serial independence in the data. Figure 6 presents the ITA distribution for the annual runoff series. The results indicate a clear increase in runoff variability under future climate forcing, particularly for the MPI-ESM-MR RCP 8.5 scenario, where several projected values are concentrated above the 1:1 reference line. This pattern suggests an amplification of high-flow conditions and greater hydrological instability under intensified radiative forcing. In contrast, the ACCESS1-0 projections exhibit a more moderate dispersion, reflecting lower variability and a less pronounced hydrological response.

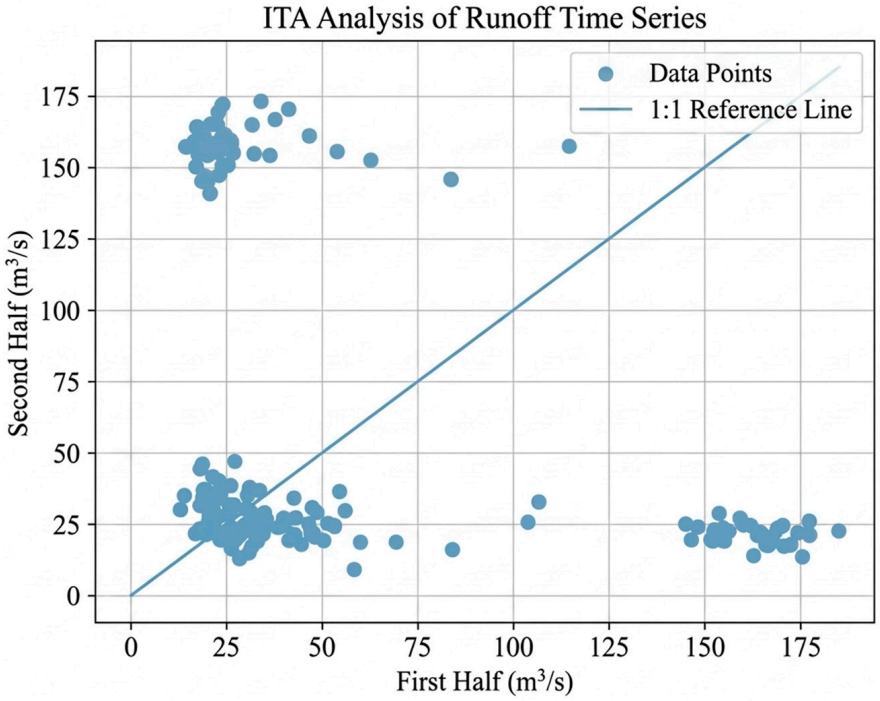

Figure 6. Innovative Trend Analysis (ITA) applied to annual runoff time series under historical and projected climate conditions.

The RAPS analysis was additionally used to evaluate cumulative deviations and structural shifts in the runoff series over time. As illustrated in Figure 7, the RAPS curves reveal alternating positive and negative anomalies throughout the analyzed period, indicating the occurrence of successive wet and dry phases within the hydrological regime of the basin. The projected series under RCP 8.5 show larger cumulative deviations compared with the historical baseline, suggesting increasing hydroclimatic irregularity toward the end of the century. These fluctuations are more pronounced in the MPI-ESM-MR simulations, confirming the strong sensitivity of runoff dynamics to projected precipitation increases and climate forcing intensity.

Overall, the combined ITA and RAPS analyses confirm that future runoff dynamics in the Ramis River basin may become increasingly irregular and non-linear under climate change scenarios. These findings support the hydrological projections obtained from the SWAT model and reinforce the importance of incorporating temporal variability analyses into long-term water resource assessments in high-Andean basins.

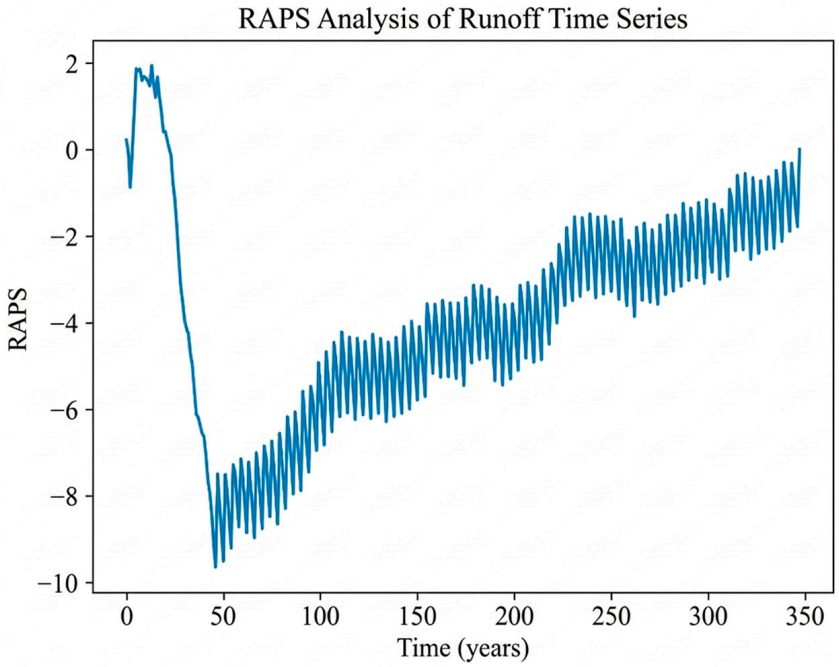

Figure 7. Rescaled Adjusted Partial Sums (RAPS) analysis showing temporal variability and structural changes in annual runoff series.

3.6. Percolation Simulation in the Aquifer

After examining the response of surface runoff under different climate scenarios, we proceeded to evaluate the evolution of percolation and groundwater discharge as key elements of the water balance in the Ramis River basin. Figure 8 presents the simulated variations for the historical baseline and the projected climate forcing scenarios. During the historical period, groundwater recharge reached 953 Mm^3, while groundwater discharge was estimated at 571.8 Mm^3. Under future climate projections, both variables show a marked increase compared with the historical reference. In the MPI-ESM-MR model, groundwater recharge increases to 1990.1 Mm^3 under the RCP 4.5 scenario and rises further to 2626.7 Mm^3 under RCP 8.5. Correspondingly, groundwater discharge increases to 1194.1 Mm^3 and 1576 Mm^3, respectively. This pattern suggests a substantial intensification of subsurface hydrological fluxes under stronger radiative forcing. A similar trend is observed in the ACCESS1-0 model, although with lower magnitudes. Recharge is projected to reach 1941 Mm^3 under RCP 4.5 and 1955.55 Mm^3 under RCP 8.5, while groundwater discharge increases to 1164.6 Mm^3 and 1173.3 Mm^3. Compared with the MPI-ESM-MR simulations, ACCESS1-0 indicates a more moderate hydrological response, highlighting structural differences between climate models in representing future precipitation and infiltration processes. Overall, the results indicate that groundwater dynamics in the Ramis River basin are highly sensitive to projected climate forcing. The strongest increase occurs under the MPI-ESM-MR model in the RCP 8.5 scenario (Table 7), suggesting that high-emission trajectories may significantly intensify groundwater recharge and baseflow contributions. The apparent simultaneous increase in surface runoff and groundwater recharge may seem contradictory; however, this behavior can be explained by precipitation intensity and temporal distribution. Under high-emission scenarios, intense rainfall events can generate rapid surface runoff while also enhancing infiltration processes, particularly in permeable zones.

Although increasing temperature tends to enhance evapotranspiration, the magnitude of precipitation increase under certain scenarios exceeds these losses, resulting in a net positive water balance. Therefore, the concurrent increase in runoff and recharge reflects

a physically plausible hydrological response rather than a model artifact. These results underline the importance of incorporating multiple climate models when evaluating future groundwater availability and hydrogeological resilience in high-altitude Andean basins.

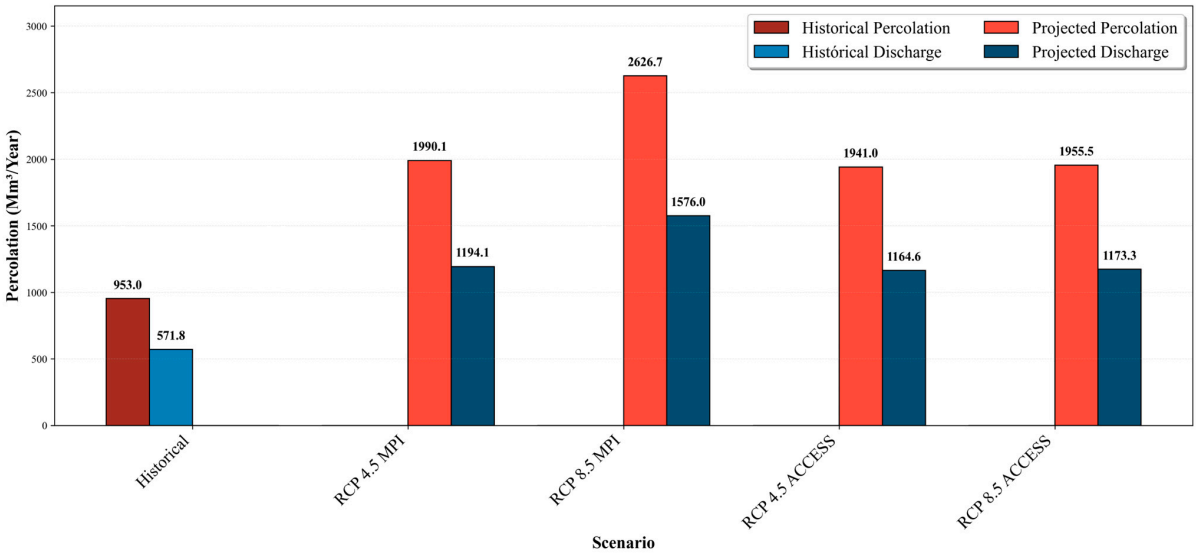

Figure 8. Groundwater recharge and discharge under climate scenarios.

In general terms, the projected increase in groundwater recharge and discharge reflects an intensification of subsurface hydrological processes under future climate scenarios. However, rising temperatures and enhanced evapotranspiration may reduce effective water availability, introducing uncertainty in the long-term sustainability of aquifer systems. This evolving hydroclimatic context poses critical challenges for water resource management in the region, requiring adaptive strategies that consider both increased hydrological variability and potential water stress conditions.

3.7. Modeling and Quantification of Renewable Water Resources (RHRs)

Figure 9 shows the modeled variation in Renewable Water Resources (RHRs) under historical conditions and future climate projections using the MPI-ESM-MR and ACCESS1-0 models for RCP 4.5 and RCP 8.5 scenarios during the period 2025–2100. The quantitative values used in this analysis are summarized in Table 8.

Table 8. Simulation of aquifer percolation under the climate scenarios examined.

Model	Scenario	Period	Groundwater Recharge (Mm^3)	Discharge (Mm^3)
Historical			953	571.8
MPI-ESM-MR	RCP 4.5	2025–2100	1990.1	1194.1
MPI-ESM-MR	RCP 8.5	2025–2100	2626.7	1576
ACCESS1-0	RCP 4.5	2025–2100	1941	1164.6
ACCESS1-0	RCP 8.5	2025–2100	1955.55	1173.3

Under historical conditions (1991–2024), the basin presents an RHR of 3669 Mm^3 $year^{-1}$, which represents the reference baseline for comparison. Future projections indicate contrasting responses depending on the climate model and emission scenario. For the RCP 4.5 scenario, both MPI-ESM-MR and ACCESS1-0 estimate a reduction in renewable water resources, reaching values close to 2831 Mm^3 $year^{-1}$, while the MPI simulation shows a slightly lower value of 2173 Mm^3 $year^{-1}$, indicating a moderate decline relative to the historical period. In the RCP 8.5 scenario, the ACCESS1-0 model projects a value of 2861 Mm^3 $year^{-1}$, suggesting a relatively stable behavior compared to RCP 4.5, whereas the

MPI-ESM-MR model produces a markedly higher estimate of 8229 Mm^3 $year^{-1}$, indicating a strong increase in renewable water availability under high-emission conditions. This large difference reflects the uncertainty associated with climate model structure and precipitation sensitivity, which significantly influences recharge and runoff processes.

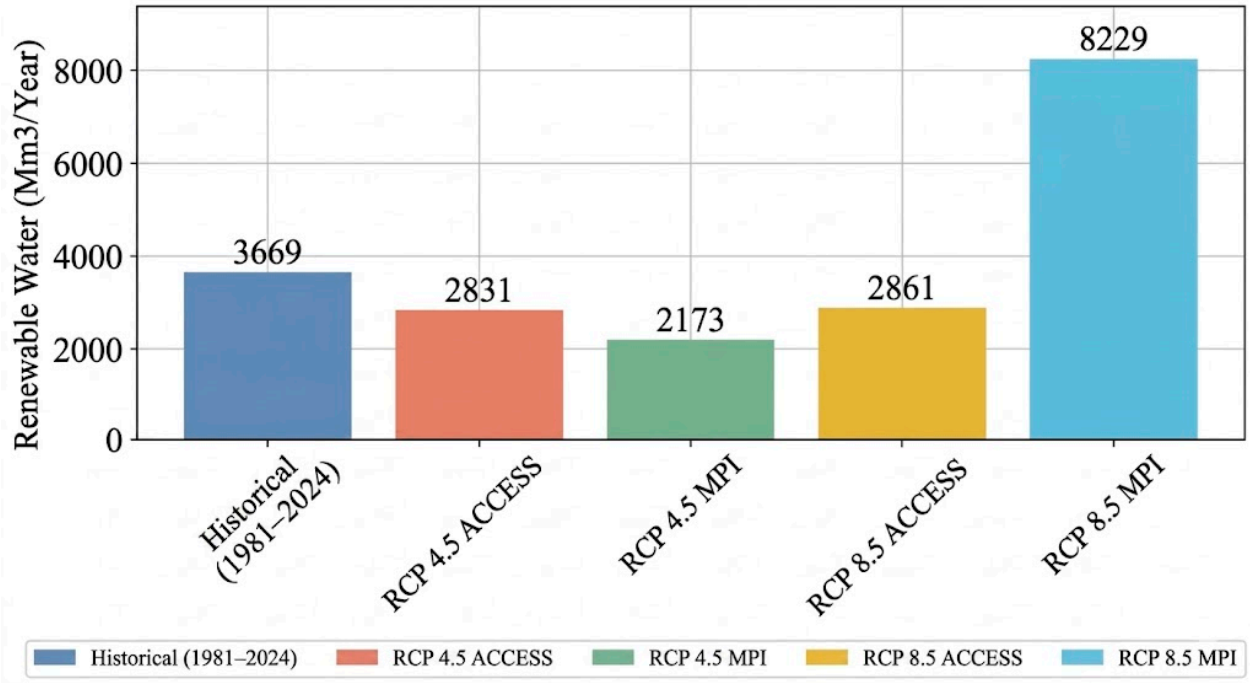

Figure 9. Projected renewable water resources under CMIP5 climate scenarios in the Ramis River basin.

Overall, the results presented in Figure 9 and Table 9 demonstrate that future RHR in the basin is highly dependent on the selected climate model, with moderate decreases under RCP 4.5 and a wide range of responses under RCP 8.5, highlighting the importance of using multiple models to properly quantify hydrological uncertainty in long-term water resource assessments.

Table 9. Simulation of renewable water under the climate scenarios examined.

Model	Scenario	Period	(RHR) (Mm^3)
	Historical		3669
MPI-ESM-MR	RCP 4.5	2025–2100	2831
MPI-ESM-MR	RCP 8.5	2025–2100	8229
ACCESS1-0	RCP 4.5	2025–2100	2831
ACCESS1-0	RCP 8.5	2025–2100	2861

3.8. Analysis of Severity Thresholds Using the SPI

The analysis of the Standardized Precipitation Index (SPI) shows that the Ramis River basin has experienced high hydroclimatic variability during the historical period, with alternating wet and dry phases as shown in Figures 10 and 11. However, future projections indicate an increase in the frequency and persistence of negative SPI values, particularly under high-emission scenarios. In the MPI-ESM-MR simulations, the RCP 8.5 scenario presents greater amplitude in SPI fluctuations, with more frequent drought events exceeding −1.5 and occasional extreme values below −2. The ACCESS1-0 model shows a more moderate pattern, although negative anomalies become more recurrent after mid-century. These results suggest that drought conditions may become more persistent

toward the end of the twenty-first century, even in scenarios where annual precipitation does not show a clear decreasing trend. This behavior is consistent with the increase in temperature projected for the region, which enhances evapotranspiration and reduces effective soil moisture.

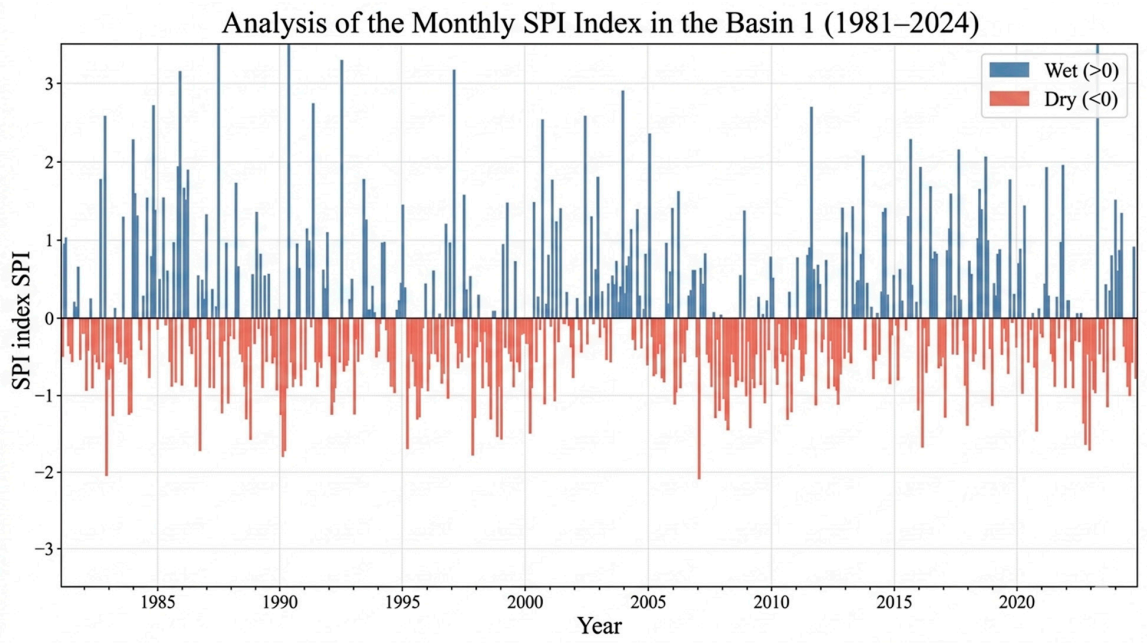

Figure 10. Time series graph of the monthly SPI: Identification of critical drought thresholds and periods of water surplus under historical climate variability.

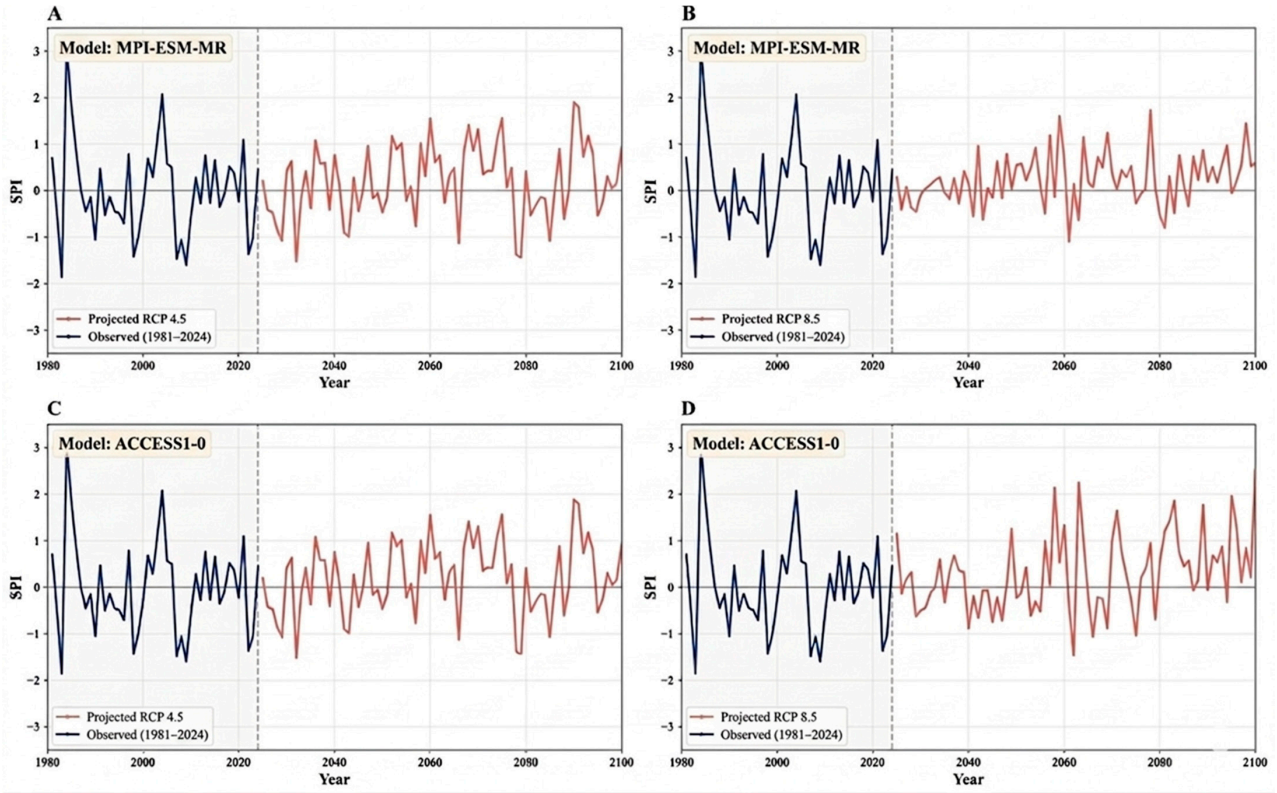

Figure 11. Evaluation of the hydrological response under future climate scenarios: (**A**) MPI-ESM-MR model under the RCP 4.5 scenario; (**B**) MPI-ESM-MR model under the RCP 8.5 scenario; (**C**) ACCESS1-0 model under the RCP 4.5 scenario; and (**D**) ACCESS1-0 model under the RCP 8.5 scenario for the period 2017–2100.

An increase in drought frequency may have significant implications for the basin. Reduced precipitation and lower soil moisture can affect crop yields, pasture productivity, and water supply for rural populations. In high-Andean environments, where water storage capacity is limited, prolonged dry periods may also reduce wetland extent and affect ecosystem services that regulate the hydrological cycle. These findings indicate that drought risk should be considered a key factor in future water planning in the Ramis basin. Monitoring systems, improved water storage infrastructure, and protection of recharge areas may be necessary to reduce the impacts of climate variability on local communities and productive systems.

4. Discussion

The results obtained in this study indicate that the hydrological response of the Ramis River basin under future climate scenarios is highly sensitive to the selection of the global climate model and emission pathway. The contrasting behavior observed between MPI-ESM-MR and ACCESS1-0 simulations confirms that uncertainty in precipitation projections remains one of the main sources of variability in hydrological impact assessments. Similar findings have been reported in recent climate–hydrology studies, where runoff projections differ significantly depending on the structure of the climate model rather than the emission scenario itself [3,4,14]. This behavior is particularly evident in high-altitude basins, where small changes in precipitation can produce large variations in runoff and groundwater recharge due to the limited storage capacity of mountain hydrological systems.

The projected reductions in runoff and renewable water resources under several scenarios are consistent with studies conducted in semi-arid and mountainous regions, which indicate that increasing temperature may enhance evapotranspiration losses and reduce effective water availability even when total precipitation does not decrease substantially [11,17]. In high-Andean environments, this effect can be intensified by strong altitudinal gradients and seasonal precipitation regimes, which control the timing of infiltration and baseflow generation. Previous applications of the SWAT model in similar basins have shown that groundwater-dominated systems are especially vulnerable to warming conditions, since increased evapotranspiration reduces soil moisture and limits aquifer recharge [20,31].

A key feature of the results is the strongly non-linear hydrological response observed between RCP 4.5 and RCP 8.5 scenarios, particularly in the MPI-ESM-MR model. While RCP 4.5 leads to a substantial reduction in runoff, RCP 8.5 produces a marked increase exceeding 130%, indicating a complete reversal of the hydrological trend. This non-linear behavior can be explained by threshold-driven processes typical of high-altitude basins. Under moderate climate forcing (RCP 4.5), temperature increases enhance evapotranspiration, reducing effective water availability and limiting runoff generation. However, under stronger forcing (RCP 8.5), the substantial increase in precipitation exceeds evapotranspiration losses, leading to rapid soil saturation and a disproportionate increase in surface runoff. Such threshold responses highlight the sensitivity of the basin to the magnitude of climate forcing and explain why hydrological changes are not proportional to emission scenarios. This mechanism is consistent with the observed transition from water-limited to precipitation-dominated conditions.

On the other hand, the extreme increase in runoff simulated by the MPI-ESM-MR model under the RCP 8.5 scenario suggests that future hydrological regimes may also be characterized by greater variability and more frequent extreme events. This result agrees with recent CMIP-based studies indicating that high-emission scenarios may intensify both drought and flood risks within the same watershed due to changes in precipitation intensity and atmospheric circulation patterns [13,14]. Such non-linear responses have been

reported in tropical and subtropical basins, where climate change can produce alternating periods of water deficit and excessive runoff, complicating water resource management and infrastructure planning.

The SPI analysis confirms that drought frequency may increase toward the end of the century, particularly under high-emission scenarios, even in cases where annual precipitation does not show a clear decreasing trend. This pattern has been observed in several recent studies, which indicate that rising temperatures can intensify drought severity through higher atmospheric water demand and reduced soil moisture availability [1,9,13]. In high-Andean basins, where wetlands, shallow aquifers, and seasonal flows play a key role in maintaining water supply, prolonged dry periods may significantly affect agricultural productivity, livestock activities, and ecosystem stability.

Additional time series analyses using the Innovative Trend Analysis (ITA) and Rescaled Adjusted Partial Sums (RAPS) methods provided further evidence of the non-linear and irregular hydrological behavior projected for the Ramis River basin under future climate scenarios. The ITA results revealed an amplification of high-flow conditions and increased dispersion in projected runoff values, particularly under the MPI-ESM-MR RCP 8.5 scenario, indicating greater hydrological variability under intensified climate forcing. Similarly, the RAPS analysis identified cumulative anomalies and structural shifts in runoff dynamics throughout the analyzed period, reflecting alternating wet and dry phases and increasing temporal instability in the basin. These findings reinforce the interpretation that future hydrological responses in the Ramis River basin may become increasingly complex and non-linear, especially under high-emission scenarios. The integration of ITA and RAPS analyses complements the SWAT-based simulations by providing additional insight into long-term variability, structural changes, and trend behavior in runoff time series.

Overall, the combined analysis of runoff, groundwater recharge, renewable water resources, and SPI variability suggests that the Ramis River basin may face a dual hydroclimatic risk during the twenty-first century. Some scenarios indicate progressive reduction in water availability, while others project increases in extreme runoff, highlighting the need to consider multiple climate models in future assessments. These results support previous research emphasizing that adaptation strategies in mountain basins should incorporate uncertainty ranges rather than relying on a single climate projection [4,20,41]. Strengthening watershed management, protecting recharge zones, improving water storage systems, and integrating climate projections into regional planning are essential measures to reduce future vulnerability in the northern Altiplano.

These findings reinforce the need to evaluate hydrological processes at the basin scale, as regional differences can significantly influence water balance components. Unlike other Andean basins, the Ramis River basin exhibits a distinct response driven by its climatic variability and physiographic conditions, emphasizing the limitations of generalizing results across different catchments.

It is important to acknowledge that the climate projections used in this study are based on CMIP5 models, which have been largely superseded by CMIP6 in recent climate research. While CMIP5 datasets remain widely used and compatible with hydrological modeling frameworks such as SWAT, they may present limitations in representing extreme climate variability.

In particular, CMIP5 models can exhibit biases in precipitation intensity and temperature variability, which may influence hydrological projections. For instance, the strong increase in runoff simulated by the MPI-ESM-MR model under the RCP 8.5 scenario may be partially associated with an overestimation of precipitation intensity, while the ACCESS1-0 model may reflect a different sensitivity to evapotranspiration processes due to its representation of temperature dynamics. Therefore, while the results provide valuable insights into

potential future hydrological responses, they should be interpreted within the context of model uncertainty. Future research should incorporate CMIP6 projections and multi-model ensembles to improve robustness and reduce uncertainty in climate impact assessments in high-Andean basins.

5. Conclusions

The hydrological simulations conducted using the SWAT model demonstrate a reliable representation of the hydrological dynamics of the Ramis River basin, as confirmed by the satisfactory calibration and validation metrics obtained for the historical period. The model results indicate that climate change may significantly modify the hydrological balance of this high-Andean basin during the twenty-first century.

The projections show that the hydrological response of the basin is highly dependent on the climate model used. Under the MPI-ESM-MR model, extreme increases in runoff are projected in the RCP 8.5 scenario, whereas substantial reductions are observed in the RCP 4.5 scenario. In contrast, the ACCESS1-0 model generally projects decreases in annual runoff and renewable water resources. Most scenarios therefore suggest a contraction in water availability compared with the historical baseline, indicating a potential increase in water scarcity conditions in the basin.

The reduction in renewable water resources and the projected increase in drought frequency identified through the SPI analysis suggest that future hydroclimatic conditions may intensify water stress in the region. Lower runoff and reduced effective recharge may limit water availability for agriculture, livestock production, and domestic supply in rural communities of the northern Altiplano. In addition, prolonged drought periods may affect high-Andean wetlands and ecological systems that depend on seasonal water flows. From a water management perspective, these results highlight the importance of incorporating climate change projections into regional planning processes. Strengthening watershed management, protecting groundwater recharge zones, improving water storage infrastructure, and implementing climate-resilient agricultural practices are key measures to reduce vulnerability to future hydroclimatic variability.

Overall, the findings indicate that the Ramis River basin may face a dual hydroclimatic risk in the coming decades, characterized by both potential water deficits and increasing hydrological extremes. Considering these uncertainties, the use of multi-model climate projections becomes essential for supporting adaptive water governance and ensuring long-term water security in high-Andean basins. This study highlights the importance of basin-specific analyses in understanding hydrological responses to climate change, demonstrating that even within the same geographic region, different basins may exhibit contrasting behaviors under similar climate forcing scenarios.

Author Contributions: J.H.M. and B.P.C.C.; methodology, J.H.M.; software, J.H.M.; validation, J.H.M., B.P.C.C. and Y.T.P.A.; formal analysis, J.H.M.; investigation, J.H.M.; resources, B.P.C.C.; data curation, J.H.M.; writing—original draft preparation, J.H.M.; writing—review and editing, B.P.C.C., Y.T.P.A., J.M.T.H., H.P.V. and M.E.C.H.; visualization, J.H.M.; supervision, B.P.C.C.; project administration, B.P.C.C.; funding acquisition, B.P.C.C. All authors have read and agreed to the published version of the manuscript.

Funding: This research received no external funding.

Data Availability Statement: The datasets used in this study were obtained from public national institutions in Peru, including the National Service of Meteorology and Hydrology (SENAMHI) and the National Water Authority (ANA). These datasets are subject to institutional regulations and therefore cannot be fully deposited in a public repository. However, they can be made available by the corresponding author upon reasonable request for academic and research purposes.

Acknowledgments: The authors acknowledge the support of the Universidad Nacional de Juliaca during the development of this study.

Conflicts of Interest: The authors declare no conflicts of interest.

References

1. Kang, S.; Kim, H.J.; Lee, J.H.; Yoon, H.C.; Kwon, H.H. Introducing a novel Standardized Precipitation Evaporation Differential Index (SPEDI) for improved flash drought detection and assessment: A case study in South Korea. *Stoch. Environ. Res. Risk Assess.* **2025**, *39*, 5601–5624. [CrossRef]
2. Sakellariou, S.; Spiliotopoulos, M.; Alpanakis, N.; Faraslis, I.; Sidiropoulos, P.; Tziatzios, G.A.; Karoutsos, G.; Dalezios, N.R.; Dercas, N. Spatiotemporal Drought Assessment Based on Gridded Standardized Precipitation Index (SPI) in Vulnerable Agroecosystems. *Sustainability* **2024**, *16*, 1240. [CrossRef]
3. Liu, T.; Liu, Y.; Si, Z.; Wang, L.; Zhao, Y.; Wang, J. Future Streamflow and Hydrological Drought Under CMIP6 Climate Projections. *Atmosphere* **2025**, *16*, 691. [CrossRef]
4. Xiao, F.; Wu, Y.; Wang, X.; Wang, P.; Fu, C.; Zhang, J. Integrated Assessment of Climate-Driven Streamflow Changes in a Transboundary Lake Basin Using CMIP6-SWAT+-BMA: A Sustainability Perspective. *Sustainability* **2025**, *17*, 7901. [CrossRef]
5. Mwinjuma, M.; Wang, R.; Mtupili, M.; Twaha, M. Comparisons of SPI and SPEI in capturing drought dynamics: A global assessment across arid and humid regions. *Atmos. Res.* **2025**, *331*, 108672. Corrigendum in *Atmos. Res.* **2026**, *329*, 108475. https://doi.org/10.1016/j.atmosres.2025.108672. [CrossRef]
6. Poudel, U.; Adhikari, S.; Karki, S.; Regmi, R.K. Climate change and hydropower resilience: A CMIP6-SWAT analysis of the Kankai River Basin's energy landscape. *H2Open J.* **2025**, *8*, 465–490. [CrossRef]
7. Dharmarathne, G.; Waduge, A.O.; Bogahawaththa, M.; Rathnayake, U.; Meddage, D.P.P. Adapting cities to the surge: A comprehensive review of climate-induced urban flooding. *Results Eng.* **2024**, *22*, 102123. [CrossRef]
8. Zeleňáková, M.; Abd Elhamid, H.; Soľáková, T.; Purcz, P.; de Michele, C.; Blišťan, P.; Hlavatá, H.; Simonová, D.; Portela, M.M. Assessment of meteorological and hydrological droughts in the eastern Slovakia using SPI and SSI indices. *Model. Earth Syst. Environ.* **2025**, *11*, 253. [CrossRef]
9. Aldhafeeri, A.A.; Ali, M.; Khan, M.; Labban, A.H. SPI-Informed Drought Forecasts Integrating Advanced Signal Decomposition and Machine Learning Models. *Water* **2025**, *17*, 2747. [CrossRef]
10. Mungul, V.; Nowbuth, M.D. Comparative study of SPI and SPEI drought indices for meteorological drought assessment in Mauritius. *Jàmbá J. Disaster Risk Stud.* **2021**, *17*, 12. [CrossRef]
11. Abeysingha, N.S.; Ray, R.L.; Tarkegn, T.G. Future hydro-climate extremes in the cypress creek watershed in Texas under different CMIP6 scenarios. *Sustain. Water Resour. Manag.* **2025**, *11*, 107. [CrossRef]
12. Kenabatho, P.K. Innovative trend analysis of long-term spatial-temporal rainfall patterns over Botswana: Implications for water resources management. *J. Hydrol. Reg. Stud.* **2025**, *58*, 102217. [CrossRef]
13. Merz, N.; Zachariah, M. Understanding droughts under climate change in South America based on severity-duration-frequency curves and drought atlases. *Clim. Change* **2025**, *178*, 163. [CrossRef]
14. Marshall, S.R.O.; Tran, T.N.D.; Arshad, A.; Rahman, M.M.; Lakshmi, V. SWAT and CMIP6-driven hydro-climate modeling of future flood risks and vegetation dynamics in the White Oak Bayou Watershed, United States. *Earth Syst. Environ.* **2025**, *10*, 553–575. [CrossRef]
15. Krichak, S.O.; Alpert, P. The role of the Near East surface pressure variations in recent past trends of wet season precipitation in the Levant. *Int. J. Climatol.* **2022**, *42*, 7103–7116. [CrossRef]
16. Janjić, J.; Tadić, L. Fields of Application of SWAT Hydrological Model—A Review. *Earth* **2023**, *4*, 331–344. [CrossRef]
17. Aloui, S.; Mazzoni, A.; Elomri, A.; Aouissi, J.; Boufekane, A.; Zghibi, A. A review of Soil and Water Assessment Tool (SWAT) studies of Mediterranean catchments: Applications, feasibility, and future directions. *J. Environ. Manag.* **2023**, *326*, 116799. [CrossRef] [PubMed]
18. Kebede, M.H.; Ahmed, A.M.; Birhan, D.A.; Damot, G.A.; Legesse, S.A. Projections of Precipitation and Temperature Changes and Trends Using CMIP6 Global Climate Models in the Eastern Amhara, Northeastern, Ethiopia. *Meteorol. Appl.* **2026**, *33*, e70145. [CrossRef]
19. Van Loon, A.F.; Laaha, G. Hydrological drought severity explained by climate and catchment characteristics. *J. Hydrol.* **2015**, *526*, 3–14. [CrossRef]
20. Dinku, M.B.; Gibre, A.M. Comparison of bias correction methods to regional climate model simulations for climate change projection in Muger Subbasin, Upper Blue Nile Basin, Ethiopia. *J. Water Clim. Change* **2024**, *15*, 2612–2627. [CrossRef]
21. Fischer, A.P.; Paveglio, T.; Carroll, M.; Murphy, D.; Brenkert-Smith, H. Assessing social vulnerability to climate change in human communities near public forests and grasslands: A framework for resource managers and planners. *J. For.* **2013**, *111*, 357–365. [CrossRef]

22. Alvar, C.; Lavado-casimiro, W.; Huerta, A.; Fernandez, C.; Vega, F.; Sabino, E.; Felipe-Obando, O. *Uso del Producto Grillado PISCO de Precipitación en Estudios, Investigaciones y Sistemas Operacionales de Monitoreo y Pronóstico Hidrometeorológico*; Servicio Nacional de Meteorología e Hidrología del Peru: Lima, Peru, 2017; Volume 1.
23. Arnold, J.G.; Srinivasan, R.; Muttiah, R.S.; Williams, J.R. Large area hydrologic modeling and assessment part I: Model development. *J. Am. Water Resour. Assoc.* **1998**, *34*, 73–89. [CrossRef]
24. Rowshon, M.K.; Dlamini, N.S.; Mojid, M.A.; Adib, M.N.M.; Amin, M.S.M.; Lai, S.H. Modeling climate-smart decision support system (CSDSS) for analyzing water demand of a large-scale rice irrigation scheme. *Agric. Water Manag.* **2019**, *216*, 138–152. [CrossRef]
25. Oeurng, C.; Cochrane, T.A.; Arias, M.E.; Shrestha, B.; Piman, T. Assessment of changes in riverine nitrate in the Sesan, Srepok and Sekong tributaries of the Lower Mekong River Basin. *J. Hydrol. Reg. Stud.* **2016**, *8*, 95–111. [CrossRef]
26. Basheer, A.K.; Lu, H.; Omer, A.; Ali, A.B.; Abdelgader, A.M.S. Impacts of climate change under CMIP5 RCP scenarios on the streamflow in the Dinder River and ecosystem habitats in Dinder National Park, Sudan. *Hydrol. Earth Syst. Sci.* **2016**, *20*, 1331–1353. [CrossRef]
27. Iqbal, M.; Wen, J.; Masood, M.; Masood, M.U.; Adnan, M. Impacts of Climate and Land-Use Changes on Hydrological Processes of the Source Region of Yellow River, China. *Sustainability* **2022**, *14*, 4908. [CrossRef]
28. Anandhi, A.; Frei, A.; Pierson, D.C.; Schneiderman, E.M.; Zion, M.S.; Lounsbury, D.; Matonse, A.H. Examination of change factor methodologies for climate change impact assessment. *Water Resour. Res.* **2011**, *47*, W03501. [CrossRef]
29. Bi, D.; Dix, M.; Marsland, S.J.; Farrell, S.O.; Rashid, H.A.; Uotila, P.; Hirst, A.C.; Kowalczyk, E.; Golebiewski, M.; Sullivan, A.; et al. The ACCESS coupled model: Description, control climate and evaluation. *Aust. Meteorol. Oceanogr. J.* **2013**, *63*, 41–64. [CrossRef]
30. Giorgetta, M.A.; Jungclaus, J.; Reick, C.H.; Legutke, S.; Bader, J.; Böttinger, M.; Brovkin, V.; Crueger, T.; Esch, M.; Fieg, K.; et al. Climate and carbon cycle changes from 1850 to 2100 in MPI-ESM simulations for the Coupled Model Intercomparison Project phase 5. *J. Adv. Model. Earth Syst.* **2013**, *5*, 572–597. [CrossRef]
31. Winchell, M.; Srinivasan, R.; Di Luzio, M.; Arnold, J. ArcSWAT interface for SWAT2009 User's Guide. In *User's Guide*; Texas A&M University: College Station, TX, USA, 2010; 489p.
32. Santhi, C.; Kannan, N.; Arnold, J.G.; Di Luzio, M. Spatial calibration and temporal validation of flow for regional scale hydrologic modeling. *J. Am. Water Resour. Assoc.* **2008**, *44*, 829–846. [CrossRef]
33. Mengistu, A.G.; van Rensburg, L.D.; Woyessa, Y.E. Techniques for calibration and validation of SWAT model in data scarce arid and semi-arid catchments in South Africa. *J. Hydrol. Reg. Stud.* **2019**, *25*, 100621. [CrossRef]
34. Bennour, A.; Jia, L.; Menenti, M.; Zheng, C.; Zeng, Y.; Barnieh, B.A.; Jiang, M. Calibration and Validation of SWAT Model by Using Hydrological Remote Sensing Observables in the Lake Chad Basin. *Remote Sens.* **2022**, *14*, 1511. [CrossRef]
35. Abbaspour, K.C. SWAT-COPA 2012. Programa de Calibración e Incertidumbre SWAT—A Manual del Usuario. 2012; Volume 130. Available online: https://swat.tamu.edu/media/114860/usermanual_swatcup.pdf (accessed on 10 May 2026).
36. Servat, E.; Dezetter, A. Sélection de fonctions critères dans le cadre d%une modélisation pluie-débit en zone de savane soudanaise. *Hydrol. Sci. J.* **1991**, *36*, 307–330. [CrossRef]
37. Geza, M.; Murray, K.E.; McCray, J.E. Watershed-Scale Impacts of Nitrogen from On-Site Wastewater Systems: Parameter Sensitivity and Model Calibration. *J. Environ. Eng.* **2010**, *136*, 926–938. [CrossRef]
38. McKee, T.B.; Doesken, N.J.; Kleist, J. The Relationship of Drought Frequency and Duration to Time Scales. In *Proceedings of the Eighth Conference on Applied Climatology*; American Meteorological Society: Anaheim, CA, USA, 1993; pp. 179–184.
39. Liu, C.; Yang, C.; Yang, Q.; Wang, J. Spatiotemporal drought analysis by the standardized precipitation index (SPI) and standardized precipitation evapotranspiration index (SPEI) in Sichuan Province, China. *Sci. Rep.* **2021**, *11*, 1280. [CrossRef] [PubMed]
40. Khalilian, S.; Shahvari, N. A SWAT Evaluation of the Effects of Climate Change on Renewable Water Resources in Salt Lake Sub-Basin, Iran. *AgriEngineering* **2019**, *1*, 44–57. [CrossRef]
41. Buytaert, W.; Vuille, M.; Dewulf, A.; Urrutia, R.; Karmalkar, A.; Célleri, R. Uncertainties in climate change projections and regional downscaling in the tropical Andes: Implications for water resources management. *Hydrol. Earth Syst. Sci.* **2010**, *14*, 1247–1258. [CrossRef]

Disclaimer/Publisher's Note: The statements, opinions and data contained in all publications are solely those of the individual author(s) and contributor(s) and not of MDPI and/or the editor(s). MDPI and/or the editor(s) disclaim responsibility for any injury to people or property resulting from any ideas, methods, instructions or products referred to in the content.